

Three dimensional strain distribution of wrinkled silicon nanomembranes fabricated by rolling-transfer technique

Qinglei Guo, Miao Zhang, Zhongying Xue, Lin Ye, Gang Wang, Gaoshan Huang, Yongfeng Mei, Xi Wang, and Zengfeng Di

Citation: *Appl. Phys. Lett.* **103**, 264102 (2013); doi: 10.1063/1.4857875

View online: <https://doi.org/10.1063/1.4857875>

View Table of Contents: <http://aip.scitation.org/toc/apl/103/26>

Published by the [American Institute of Physics](#)

Articles you may be interested in

[Uniaxial and tensile strained germanium nanomembranes in rolled-up geometry by polarized Raman scattering spectroscopy](#)

AIP Advances **5**, 037115 (2015); 10.1063/1.4914916

[Exceptional transport property in a rolled-up germanium tube](#)

Applied Physics Letters **110**, 112104 (2017); 10.1063/1.4978692

[Optical properties of rolled-up tubular microcavities from shaped nanomembranes](#)

Applied Physics Letters **94**, 141901 (2009); 10.1063/1.3111813

[Mechanics of rollable and foldable film-on-foil electronics](#)

Applied Physics Letters **74**, 1177 (1999); 10.1063/1.123478

[Buckling modes of elastic thin films on elastic substrates](#)

Applied Physics Letters **90**, 151902 (2007); 10.1063/1.2720759

[Strain-induced wrinkling on SiGe free standing film](#)

Applied Physics Letters **89**, 043119 (2006); 10.1063/1.2236299



Scilight

Sharp, quick summaries **illuminating**
the latest physics research

Sign up for **FREE!**

AIP
Publishing

Three dimensional strain distribution of wrinkled silicon nanomembranes fabricated by rolling-transfer technique

Qinglei Guo,¹ Miao Zhang,¹ Zhongying Xue,¹ Lin Ye,¹ Gang Wang,¹ Gaoshan Huang,² Yongfeng Mei,^{2,a)} Xi Wang,¹ and Zengfeng Di^{1,a)}

¹State Key Laboratory of Functional Materials for Informatics, Shanghai Institute of Microsystem and Information Technology, Chinese Academy of Sciences, 865 Changning Road, Shanghai 200050, People's Republic of China

²Department of Materials Science, Fudan University, Shanghai 200433, People's Republic of China

(Received 12 November 2013; accepted 11 December 2013; published online 23 December 2013)

This paper introduces a simple transfer technique named as rolling-transfer technology to transfer Si nanomembranes to pre-stressed elastomers with nearly 100% transfer efficiency. When transferred onto the elastomeric substrate, wave-like wrinkled Si nanomembranes with uniform periodicity and amplitude are formed. The three dimensional (3-D) strain distribution of the wrinkled Si nanomembranes has been investigated in detail through the micro-Raman mapping using two excited laser wavelengths. The sinusoidal bulking geometry of Si nanomembrane results in a periodical strain alternation along x direction, while a homogenous strain distribution in y direction. The inhomogeneous strain distribution along z direction can be interpreted with the physical model considering the shift of the neutral mechanical plane, which is qualitatively determined by the Von Karman elastic nonlinear plate theory, including the bending effect and the shear forces existing at the Si nanomembrane/elastomeric substrate interface. © 2013 AIP Publishing LLC. [<http://dx.doi.org/10.1063/1.4857875>]

Complementary to traditional electronics on rigid substrate, flexible electronics have been considered as an emerging technology that could be valuable for various application, such as electronic paperlike display devices,¹⁻³ robotic sensory skins,⁴ stretchable Si integrated circuits,⁵ photovoltaics,^{6,7} and structural health monitoring devices.⁸ In order to fabricate the flexible electronics, researchers tried to transfer single-crystal semiconductor nanomembranes^{9,10} to elastomeric or plastic substrates. To further improve the flexibility of the electronic devices, wrinkled semiconductor nanomembranes¹¹ with wavy geometries were invented to accommodate large compressive or tensile strain.¹²⁻¹⁵ In addition, the accommodated strain plays an important role in the carrier mobility enhancement¹⁶ and the band structure modulation of the semiconductor materials,^{17,18} thus improving the performance and response of the devices. For instance, strains in the films such as Co films,¹⁹ Co/Cu multilayers,²⁰ graphene²¹ that originated from the stretched flexible substrate can tune the performance of the devices. Khang *et al.*¹² has demonstrated that the strain distribution of the silicon wrinkle can be analyzed by Raman measurements. However, due to the fact that the thickness of wrinkled semiconductor nanomembrane is below the spatial resolution of Raman system,²² only the planar strain distribution can be achieved, while the vertical distribution perpendicular to the deformed direction is barely studied, though the performance of the integrated flexible devices closely correlates with the 3-D strain distribution.^{17,18}

We developed an approach called rolling-transfer technique, which is more convenient and controllable compared to traditional transfer-printing method,^{12,23,24} to form

wrinkled Si nanomembranes on elastomeric substrate. Furthermore, taking advantage of the fact that Raman spectroscopy is able to probe the strain distribution along depth by using excitation with different wavelengths, the strain and its 3-D distribution in the wrinkled Si nanomembranes has been comprehensively investigated, and a relevant theoretical model has been proposed.

The detailed process for rolling-transfer technique is illustrated in Fig. 1. First, a (100) silicon-on-insulator (SOI) wafer with a 30 nm top Si nanomembrane and 340 nm buried oxide (BOX) layer was patterned into rectangles ($30 \times 120 \mu\text{m}^2$), as shown in Fig. 1(a). The patterned SOI wafer was then dipped into HF solution to release top Si nanomembranes [Fig. 1(b)]. Facilitated by van der Waals forces,²⁵ the free-standing nanomembranes were supported by, but not bonded to the underlying substrate without altering the pattern pre-defined [Fig. 2(a)]. Then, the cured polydimethylsiloxane (PDMS) stamp was bonded on a rigid steel cylinder and put into conformal contact with the free-standing Si nanomembranes, as shown in Fig. 1(b). As the rolling of the steel cylinder proceeded, the silicon nanomembranes were detached from the Si substrate and transferred on to the pre-stressed PDMS surface [Fig. 1(c)]. Finally, PDMS was removed from the cylinder and restored into the flat geometry, thus creating the wrinkle-shaped single-crystal Si nanomembranes [Fig. 1(d)]. Superior to traditional transfer-printing method,^{12,23,24} the proposed rolling-transfer technique can preclude the intractable bubble formation between PDMS and Si nanomembranes, during the conformal contact process, therefore, the transfer efficiency can be significantly enhanced up to $\sim 100\%$. In addition, the geometry including the amplitude and the wavelength of wrinkle-shaped single-crystal Si nanomembranes can be precisely tuned by the radius of the steel cylinder (not shown). The optical microscope image of wrinkled Si

^{a)}Authors to whom correspondence should be addressed. Electronic addresses: yfm@fudan.edu.cn and zfdi@mail.sim.ac.cn.

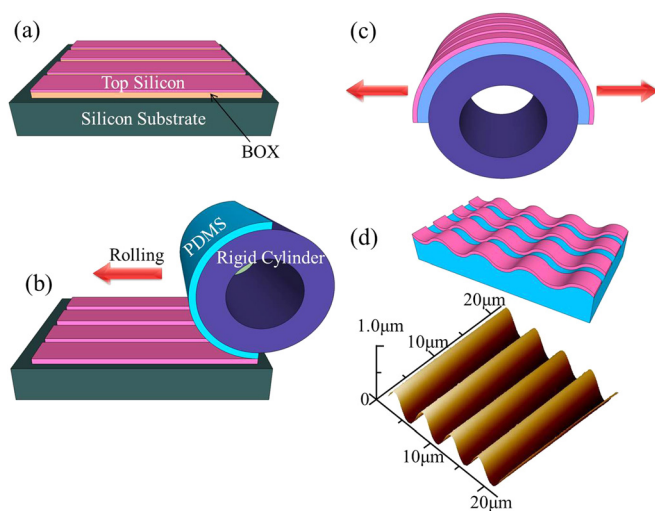


FIG. 1. Schematic illustration of the process for forming silicon wrinkles on pre-stressed elastomers.

nanomembranes on PDMS is exhibited in Fig. 2(b). Beside two flat ends are observed,²⁶ the majority region of Si nanomembrane has transformed into wavy shape. From the angled-plan view scanning electron microscope (SEM) image shown in Fig. 2(c), it is observed that wrinkled nanomembranes show regular wave-like structures consisting periodic geometry with uniform wavelength (λ). In addition, cross-sectional SEM image (dotted white line cut along the wrinkle displayed in Fig. 2(c) in the inset of Fig. 2(c) suggests that good adhesion between nanomembranes and PDMS, either at the crest or at the valley, and no air-gap is observed at the interface.

Section analysis by means of line-cuts from atomic force microscope (AFM) image of wrinkled nanomembranes provides a quantitative measure of the periodic geometry, as shown in Fig. 2(d). The result indicates that the wrinkles are sinusoidal, with a wavelength (λ) of $6.55 \mu\text{m}$ and an

amplitude (A) of $\sim 580 \text{ nm}$ at the middle, propagate symmetrically to the two ends, and finally reaches the stable configuration.²⁷

To further explore the 3-D strain distribution in the wrinkled Si nanomembrane, micro-Raman mapping measurements on wrinkled nanomembrane using 514 nm line of Ar^+ laser and 325 nm line of He-Cd laser as light sources have been performed. A typical color-coded Raman peak (Si-Si TO phonon) position extracted from the mappings under the excitation of the lasers with two different wavelengths (514 nm and 325 nm) are shown in Figs. 3(a) and 3(b), respectively. The peak position, which is associated with the strain status at the point probed, shows periodic alternation along the x direction while keeps constant along the y direction. Furthermore, in order to determine the correspondence between two Raman mappings, the measured region includes the wrinkled Si nanomembrane area, the flat Si nanomembrane area, and the PDMS area (displayed in Fig. 2(b) with the white dotted rectangle), so the edge of Si nanomembrane can be used as reference mark to align two separate Raman mappings. It is striking to observe that the positions of the crest lines (the maximum wavenumber) of Raman mapping measured by 514 nm laser exactly correspond to the valley lines (the minimum wavenumber) of the counterpart obtained by 325 nm laser. Due to the fact that the strain distribution along y direction is homogeneous, the analysis of Raman mapping can be simplified by the line-cut along x direction from the mapping, as shown in Figs. 3(c) and 3(d). The micro-Raman measurements of the Si peak as a function of distance along the Si nanomembranes present the typical sinusoidal shape, which is consistent with a computed fit to a sine function, as shown by the solid line. The periodicity of peak position along x direction is similar to that obtained from AFM image (Fig. 2(d)). For the strain distribution profile obtained with 514 nm laser, $\omega_{\text{bulk}} = 520.7 \text{ cm}^{-1}$, which corresponds to unstrained bulk Si, is found to locate around the middle of the sinusoidal curve

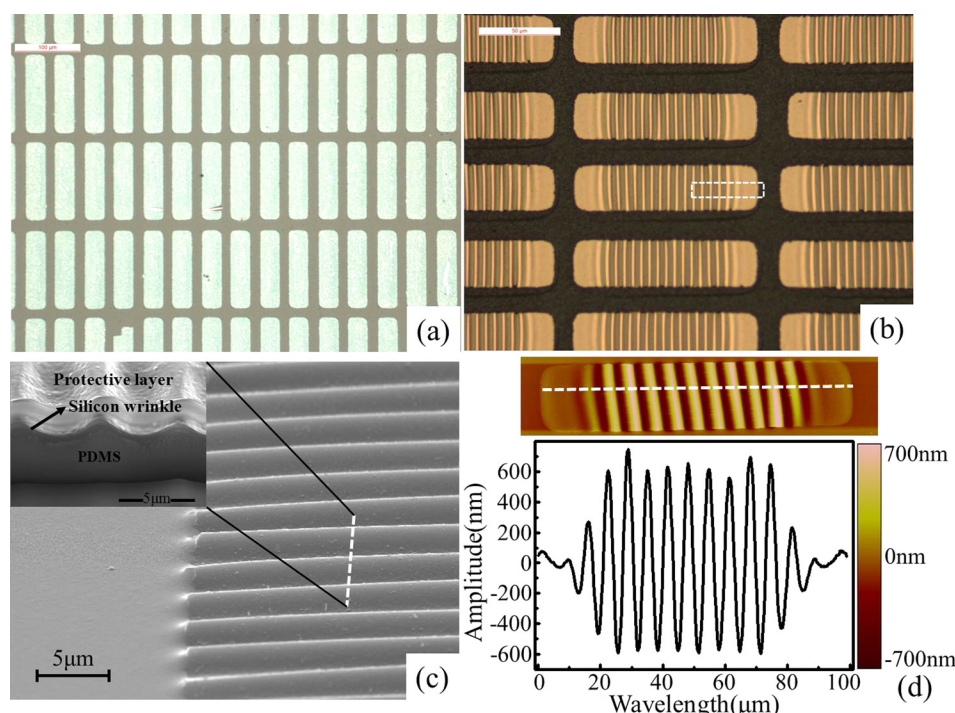


FIG. 2. Morphologies of Si nanomembranes: (a) Optical microscopy image showing the free-standing Si nanomembranes attached to silicon substrate, and the scale bar is $100 \mu\text{m}$; (b) optical microscopy image of wrinkled silicon nanomembranes, and the scale bar is $50 \mu\text{m}$. The rectangle region indicated by the dotted line is subsequently measured by Raman mapping; (c) SEM image of wrinkled Si nanomembranes; (d) AFM and section analysis of wrinkled Si nanomembranes.

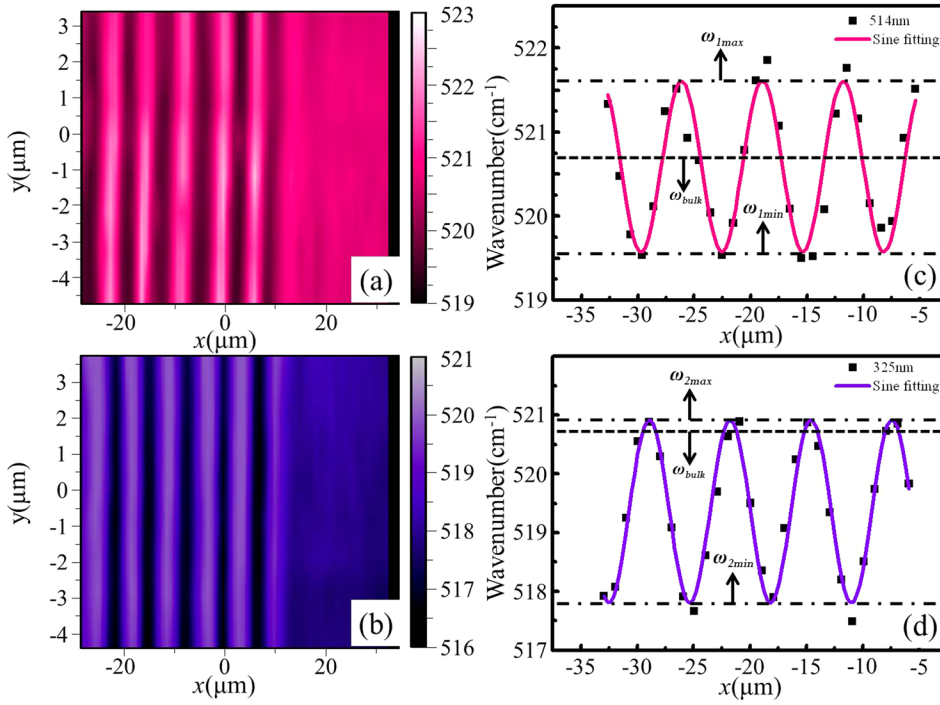


FIG. 3. Micro-Raman mapping measurements of the wrinkled Si nanomembranes, and the corresponding section analysis: (a) and (c) 514 nm laser; (b) and (d) 325 nm laser.

(see dotted line in Fig. 3(c)). The maximum wavenumber from TO Raman peak (ω_{1max}) at the crest of the wrinkle is greater than ω_{bulk} , while the minimum wavenumber (ω_{1min}) at the valley of the wrinkle is less than ω_{bulk} . However, when changed to 325 nm laser (Fig. 3(d)), the maximum wavenumber (ω_{2max}) decreases significantly and is approaching ω_{bulk} , and the minimum wavenumber (ω_{2min}) become much smaller than ω_{bulk} . Furthermore, the sine function for 325 nm laser shifts π compared to that for 514 nm laser, which consists with the crest-valley correspondence in the Raman mappings as depicted previously. Since the penetration depth, i.e., the detection depth of Raman system correlates with the wavelength of the excitation laser, it is believed that the above phase shift is due to the inhomogeneous strain distribution along the direction perpendicular to the silicon nanomembrane, i.e., z direction.

To simplify the theoretical analysis of the strain distribution along the z direction of Si nanomembrane, the entire silicon nanomembranes/PDMS substrate system is separated into two basic elements, i.e., the suspended silicon wrinkle and the unattached elastomeric PDMS substrate in wrinkled shape. For the suspended silicon wrinkle, in addition to the bending effect,^{28–30} the Von Karman elastic nonlinear plate theory^{31–33} is also integrated, so the dominant strain distribution in the deformed wrinkles is

$$\varepsilon_{xx}(x, y, z) = \varepsilon_{xx}^0 + \frac{\partial u_x}{\partial x} + \frac{1}{2} \left(\frac{\partial \omega_x}{\partial x} \right)^2 - \frac{1}{2} \frac{\partial^2 \omega_x}{\partial x^2} z, \quad (1)$$

where ε_{xx}^0 is the initial strain (the compressive strain due to the relaxation of pre-strain in PDMS, $\sim -4.87\%$ for our experiment), u_x denotes the in-plane displacements in the x direction, ω_x is the deflection of the nanomembranes which can be written as $\omega_x = A \cos(kx)$, and $k = \frac{2\pi}{\lambda}$. z is the distance from the center of the wrinkles. When $\omega_x = A \cos(kx)$ is substituted into Eq. (1), and the uniformity of the strains requires that the in-plane displacement field be written as²⁹

$$u_x = \frac{1}{8} k A^2 \sin(2kx). \quad (2)$$

Substituting $\omega_x = A \cos(kx)$ and Eq. (2) into Eq. (1), the membrane strain field is

$$\varepsilon_{xx}(x, y, z) = \varepsilon_{xx}^0 + \frac{1}{4} k^2 A^2 + \frac{1}{2} A k^2 \cos(kx) z. \quad (3)$$

For the wrinkled nanomembrane with the certain geometry, both ε_{xx}^0 and $k^2 A^2/4$ are constants, so the strain distribution is well tuned by the product of $\cos(kx)$ and z . At the crest or the valley of the wrinkled Si nanomembrane, $\cos(kx)$ is equal to $+1$ or -1 , respectively, the depth distribution of the strain varies as the value of z changes only. In the top panel of Fig. 4, the schematic side-view representation of the forces and lattice constants in the crest and the valley are shown. The tensile strain is distributed at the upper layers of crest, as marked with “+” while the compressive strain marked with “-” is distributed at the lower layers. The situation of strain distribution in the valley is opposite with the valley. In particular, a zero crossing occurs in the wrinkles referred to as the neutral mechanical plane,³⁴ which is labeled with dotted line. The position of the neutral mechanical plane relative to the center of the wrinkles can be obtained when $\varepsilon_{xx}(x, y, z) = 0$. Using the parameters of the wrinkles described above, it is found that $\varepsilon_{xx}^0 + \frac{1}{4} k^2 A^2 > 0$. Therefore, at the crest and at the valley, the positions of the neutral mechanical planes are

$$z = \begin{cases} \frac{\varepsilon_{xx}^0 + \frac{1}{4} k^2 A^2}{\frac{1}{2} A k^2} < 0, \text{ at the crest, and } \cos(kx) = 1 \\ \frac{\varepsilon_{xx}^0 + \frac{1}{4} k^2 A^2}{\frac{1}{2} A k^2} > 0, \text{ at the valley, and } \cos(kx) = -1. \end{cases} \quad (4)$$

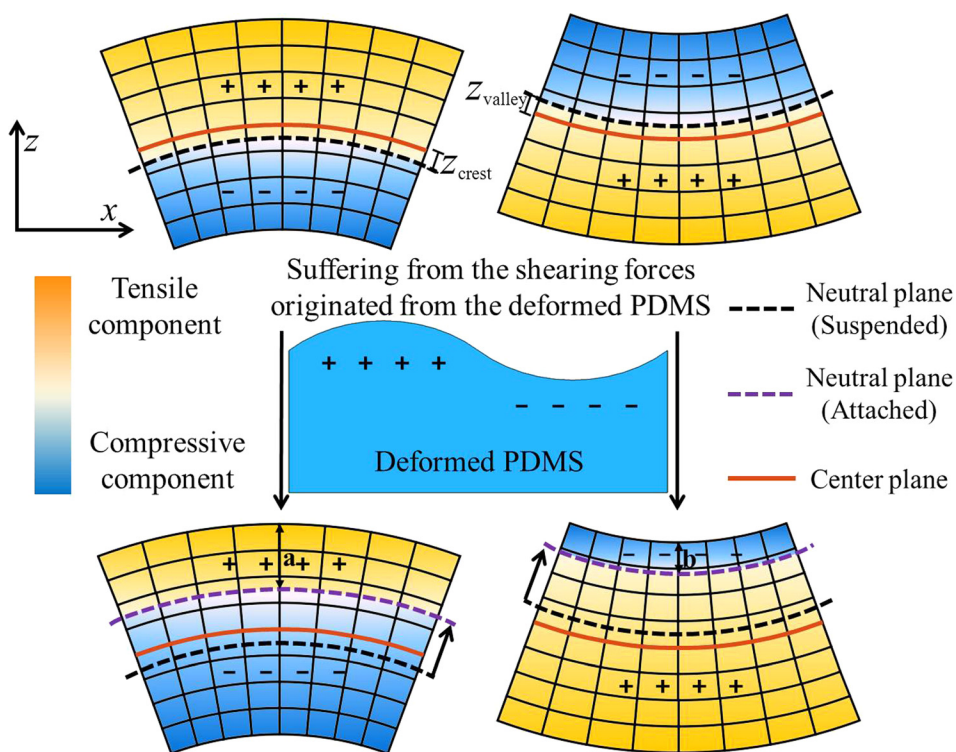


FIG. 4. Theoretical model for the strain distribution in the wrinkled silicon nanomembranes on PDMS.

For the crest, the value of z is negative, which indicates that the neutral mechanical plane is located at the position below the center of the wrinkles. While, the neutral mechanical plane moves to the positive side at the valley, as depicted in the top panel of Fig. 4.

For the independent sinusoidal elastomeric PDMS substrate whose surface has identical geometry to the wrinkles, the tensile strain is distributed at the crest, while the compressive strain exists at the valley, as schematically shown in the middle panel of Fig. 4. When the suspended silicon wrinkle is adhered to the elastomeric PDMS substrate to form the nanomembrane/PDMS system, the shearing forces at the interface provides the extra force to confine the nanomembrane in the sinusoidal shape. At the crest region of nanomembrane, the shearing forces originated from the deform PDMS act as a role of compression to squeeze the nanomembrane. While, near the valley region of nanomembrane, the expansion effect from the PDMS is exerted on the nanomembrane. Therefore, such shearing forces result in the shift of the neutral mechanical plane towards the top surfaces of nanomembrane/PDMS system. As a result, the depth of the neutral mechanical plane at the crest region is relatively larger than that at the valley region, as indicated by “a” and “b,” respectively, as shown in the bottom panel of Fig. 4. In our previous study, the position of the neutral mechanical plane, which is closely correlated with the pre-strain of PDMS, can be well depicted by the fitting program.³⁵

It should be noted that the detection depth of Raman system is determined by the wavelength of the excitation laser.³⁶ For instance, for 325 nm laser, the maximum penetration depth in Si is about 8 nm, so only 1/3 of the total thickness of Si nanomembrane contributes to the Raman signal, while for 514 nm laser, the signal from the total thickness ($D = 30$ nm) can be collected since the penetration depth of 514 nm laser in silicon (~ 680 nm) is well beyond the Si nanomembrane

thickness. At the crest region, since the neutral plane sits above the center of the nanomembrane, the average strain crossing the whole thickness is in the compressive state. Therefore, the TO mode detected by 514 nm laser should shift from ω_{bulk} to higher wavenumber (ω_{1max}), which corresponds to the maximum compressive strain. For the valley case, the tensile strain dominates, so the TO mode appears at lower wavenumber (ω_{1min}). In addition, due to the fact that the neutral mechanical plane at the crest region is relatively deeper than that at the valley region ($a > b$), the absolute value of the compressive strain existing at the crest region is larger than the counterpart tensile strain found at the valley region. Therefore, the dotted line corresponding to ω_{bulk} locates at the position slightly higher than the middle plane of the sinusoidal curve, as shown in Fig. 3(c). However, the situation becomes distinct when only the top 1/3 of Si nanomembrane is detected by 325 nm laser. At the crest region, the depth of the neutral mechanical plane, i.e., a is comparable to the maximum penetration depth of Raman system, so only the tensile strain near the top surface of silicon nanomembrane is detected and the TO mode shifts to much lower wavenumber (ω_{2min}). But, due to the fact that the neutral mechanical plane at the valley region is much shallower compared to the crest region, the 325 nm laser is capable of penetrating the neutral mechanical plane and detect the tensile strain distributed underneath. Therefore, both the compressive strain above the neutral mechanical plane and the tensile strain below can be measured, thus resulting in the TO mode (ω_{2max}) is quite close to the value corresponding to ω_{bulk} , as observed in Fig. 3(d). Furthermore, it should be noted that the Raman results obtained from the regions other than the crest area and the valley area can be interpreted by the physical model proposed here.

In summary, a simple strategy to transfer Si nanomembrane with engineered wrinkle geometry on the elastomeric

substrate has been demonstrated. The 3-D strain distribution in the wrinkle has been studied in detail by the micro-Raman mapping. Our study may provide a comprehensive understanding for the bulked thin film/elastomeric substrate system, which have many envisioned applications especially for the flexible electronics.

This work was financially supported by the National Natural Science Foundation of China under Grant Nos. 61176001, 51222211, 61274136, and 51322201, National Basic Research Program of China (973 Program) under Grant No. 2010CB832906, Pujiang Talent Project of Shanghai under Grant No. 11PJ1411700, Specialized Research Fund for the Doctoral Program of Higher Education (No. 20120071110025), Science and Technology Commission of Shanghai Municipality (No. 12520706300), Chinese Academy of Sciences (CAS) International Collaboration and Innovation Program on High Mobility Materials Engineering, and One Hundred Talent project from CAS.

- ¹S. Lee, B. Koo, J.-G. Park, H. Moon, J. Hahn, and J. M. Kim, *MRS Bull.* **31**, 455 (2006).
- ²J. A. Rogers, Z. Bao, K. Baldwin, A. Dodabalapur, B. Crone, V. R. Raju, V. Kuck, H. Katz, K. Amundson, J. Ewing, and P. Drzaic, *Proc. Natl. Acad. Sci. U.S.A.* **98**, 4835 (2001).
- ³G. H. Gelinck, H. Edzer, A. Huitema, E. Veenendaal, E. Cantatore, L. Schrijnemakers, J. B. P. H. Putten, T. C. T. Geuns, M. Beenhakkers, J. B. Giesbers, B.-H. Huisman, E. J. Meijer, E. M. Benito, F. J. Touwslager, A. W. Marsman, B. J. E. Rens, and D. M. Leeuw, *Nature Mater.* **3**, 106 (2004).
- ⁴T. Someya, Y. Kato, T. Sekitani, S. Lba, Y. Noguchi, Y. Murase, H. Kawaguchi, T. Sakurai, and G. M. Whitesides, *Proc. Natl. Acad. Sci. U.S.A.* **102**, 12321 (2005).
- ⁵D.-H. Kim, J.-H. Ahn, W. M. Choi, H.-S. Kim, T.-H. Kim, J. Song, Y. Y. Huang, Z. Liu, C. Lu, and J. A. Rogers, *Science* **320**, 507 (2008).
- ⁶J. Yoon, L. Li, A. V. Semichaevsky, J. H. Ryu, H. T. Johnson, R. G. Nuzzo, and J. A. Rogers, *Nat. Commun.* **2**, 343 (2011).
- ⁷J. Lee, J. Wu, M. Shi, J. Yoon, S.-I. Park, M. Li, Z. Liu, Y. Huang, and J. A. Rogers, *Adv. Mater.* **23**, 986 (2011).
- ⁸A. Nathan, B. Park, A. Sazonov, S. Tao, I. Chan, P. Servati, K. Karim, T. Charania, D. Striakhilev, Q. Ma, and R. V. R. Murthy, *Microelectron. J.* **31**, 883 (2000).
- ⁹J. A. Rogers, M. G. Lagally, and R. G. Nuzzo, *Nature* **477**, 45 (2011).
- ¹⁰G. Huang and Y. Mei, *Adv. Mater.* **24**, 2517 (2012).
- ¹¹Y. Mei, S. Kiravittaya, S. Harazim, and O. G. Schmidt, *Mater. Sci. Eng. R* **70**, 209 (2010).
- ¹²D.-Y. Khang, H. Jiang, Y. Huang, and J. A. Rogers, *Science* **311**, 208 (2006).
- ¹³Y. Sun, W. M. Choi, H. Jiang, Y. Y. Huang, and J. A. Rogers, *Nat. Nanotechnol.* **1**, 201 (2006).
- ¹⁴Y. Sun, V. Kumar, I. Adesida, and J. A. Rogers, *Adv. Mater.* **18**, 2857 (2006).
- ¹⁵W. M. Choi, J. Song, D.-Y. Khang, H. Jiang, Y. Huang, and J. A. Rogers, *Nano Lett.* **7**, 1655 (2007).
- ¹⁶J. Welser, J. L. Hoyt, and J. F. Gibbons, *IEEE Electron Device Lett.* **15**, 100 (1994).
- ¹⁷J. R. Jain, A. Hryciw, T. M. Baer, D. A. B. Miller, M. L. Brongersma, and R. T. Howe, *Nature Photon.* **6**, 398 (2012).
- ¹⁸M. J. Suess, R. Geiger, R. A. Minamisawa, G. Schiefler, J. Frigerio, D. Chrastina, G. Isella, R. Spolenak, J. Faist, and H. Sigg, *Nature Photon.* **7**, 466 (2013).
- ¹⁹Y. F. Chen, J. McCord, J. Freudenberger, R. Kaltofen, and O. G. Schmidt, *J. Appl. Phys.* **105**, 07C302 (2009).
- ²⁰Y.-f. Chen, Y. Mei, R. Kaltofen, J. I. Monch, J. Schumann, J. Freudenberger, H.-J. Klauß, and O. G. Schmidt, *Adv. Mater.* **20**, 3224 (2008).
- ²¹Y. Wang, R. Yang, Z. Shi, L. Zhang, D. Shi, E. Wang, and G. Zhang, *ACS Nano* **5**, 3645 (2011).
- ²²J. Chen, G. Conache, M.-E. Pistol, S. M. Gray, M. T. Borgstrom, H. Xu, H. Q. Xu, L. Samuelson, and U. Håkanson, *Nano Lett.* **10**, 1280 (2010).
- ²³E. Menard, R. G. Nuzzo, and J. A. Rogers, *Appl. Phys. Lett.* **86**, 093507 (2005).
- ²⁴M. A. Meitl, Z. Zhu, V. Kumar, K. J. Lee, X. Feng, Y. Y. Huang, I. Adesida, R. G. Nuzzo, and J. A. Rogers, *Nature Mater.* **5**, 33 (2006).
- ²⁵G. M. Cohen, P. M. Mooney, V. K. Paruchuri, and H. J. Hovel, *Appl. Phys. Lett.* **86**, 251902 (2005).
- ²⁶C. T. Koh, Z. J. Liu, D.-Y. Khang, J. Song, C. Lu, Y. Huang, J. A. Rogers, and C. G. Koh, *Appl. Phys. Lett.* **91**, 133113 (2007).
- ²⁷X. Feng, B. Qu, B. Lu, Z. Zhao, and X. Fang, *Appl. Phys. Lett.* **99**, 141903 (2011).
- ²⁸X. Chen and J. W. Hutchinson, *J. Appl. Mech.* **71**, 597 (2004).
- ²⁹Z. Y. Huang, W. Hong, and Z. Suo, *J. Mech. Phys. Solids*, **53**, 2101 (2005).
- ³⁰G.-E. Chang, C.-O. Chang, and H. Cheng, *J. Appl. Phys.* **111**, 034314 (2012).
- ³¹Z. Suo, E. Y. Ma, H. Gleskova, and S. Wagner, *Appl. Phys. Lett.* **74**, 1177 (1999).
- ³²L. D. Landau and E. M. Lifshitz, *Theory of Elasticity* (Pergamon, New York, 1986).
- ³³S. P. Timoshenko and J. M. Gere, *Theory of Elastic Stability* (McGraw-Hill, New York, 1961).
- ³⁴A. J. Baca, J.-H. Ahn, Y. Sun, M. A. Meitl, E. Menard, H.-S. Kim, W. M. Choi, D.-H. Kim, Y. Huang, and J. A. Rogers, *Angew. Chem., Int. Ed.* **47**, 5524 (2008).
- ³⁵Y. Mei, S. Kiravittaya, M. Benyoucef, D. J. Thurmer, T. Zander, C. Deneke, F. Cavallo, A. Rastelli, and O. G. Schmidt, *Nano Lett.* **7**, 1676 (2007).
- ³⁶J. Takahashi and T. Makino, *J. Appl. Phys.* **63**, 87 (1988).